Dipolarization Fronts in the Jovian Magnetotail: Statistical Survey of Ion Intensity Variations Using Juno Observations

A. Blöcker[1] , **E. A. Kronberg[1]** , **E. E. Grigorenko[2]**, **E. Roussos[3]** , and **G. Clark[4]**

[1]Department of Earth and Environmental Sciences, Ludwig Maximilian University of Munich, Munich, Germany, [2]Space Research Institute, Russian Academy of Sciences, Moscow, Russia, [3]Max Planck Institute for Solar System Research, Göttingen, Germany, [4]Johns Hopkins University, Applied Physics Laboratory, Laurel, MD, USA

Abstract Energetic particle acceleration and energization in planetary magnetotails are often associated with dipolarization fronts characterized by a rapid increase of the meridional component of the magnetic field. Despite many studies of dipolarization events in Earth's magnetotail, Jupiter's magnetotail provides an almost ideal environment to study high-energetic ion acceleration by dipolarization fronts because of its large spatial scales and plasma composition of heavy and light ions. In this study, we focus on the response of different high-energetic ion intensities (H, He, S, and O) to prominent magnetic dipolarization fronts inside the Jovian magnetotail. We investigate if ion energization and acceleration are present in the observations around the identified dipolarization fronts. Therefore, we present a statistical study of 87 dipolarization front signatures, which are identified in the magnetometer data of the Juno spacecraft from July 2016 to July 2021. For the ion intensity analysis, we use the energetic particle observations from the Jupiter Energetic Particle Detector Instrument. Our statistical study reveals that less than half of the identified events are accompanied by an increase of the ion intensities, while most of the other events show no significant change in the ion intensity dynamics. In about 40% of the events located in the dawn sector a significant decrease of the energy spectral index is detected indicating ion acceleration by the dipolarization fronts.

1. Introduction

Magnetic reconnection in planetary magnetotails might cause a magnetic field reconfiguration, acceleration, and energization of charged particles. An indicative feature of magnetic reconnection is magnetic dipolarization which is identified by a fast change of the magnetic field configuration from a stretched tail-like to a dipole-like. Dipolarization fronts (DFs) are localized pulses in the magnetic field which propagate toward the planet and are characterized by a sudden increase in the meridional component of a planetary magnetic field. They are described as the leading edge of a dipolarization signature in the meridional component of the magnetic field (e.g., Nakamura et al., 2002) and are often associated with bursty bulk flows (Angelopoulos et al., 1992; Liu et al., 2014). Dipolarization events in the Earth's near magnetotail have been extensively studied for many years by multispacecraft observations and modeling (see review of Fu et al. (2020)). However, DFs are not only limited to the Earth's magnetosphere but have been also observed at Mercury (Sundberg et al., 2012), Saturn (Jackman et al., 2015; Smith et al., 2018; Xu et al., 2021; Yao et al., 2017, 2018), and Jupiter (Kasahara et al., 2011, 2013; Kronberg et al., 2012; Vogt et al., 2020).

Strong electric fields associated with dipolarizations can be responsible for acceleration and energetic particle flux increases (e.g., Birn et al., 2013; Liu et al., 2016). It was shown that besides suprathermal electrons, energetic ions can be accelerated via reflection by the approaching DF, adiabatic processes, such as Fermi and betatron acceleration, nonadiabatic resonant interaction, and wave-particle interaction (see Fu et al., 2020, and references therein).

Studies of ion acceleration around DFs in the Earth's magnetotail are restricted, since the Earth's magnetosphere is spatially limited and contains mostly protons with a minor contribution from heavy ions. In contrast, Jupiter's giant magnetosphere provides an excellent laboratory to study the acceleration of multispecies plasma. Its magnetosphere is governed by fast planetary rotation and mass-loading from the moon Io. Iogenic ions (O^+, O^{++}, S^{++}, S^{+++}) and the solar wind ions (H^+ and He^{++}) are present in the Jovian magnetosphere. The plasma flow is corotationally dominated (e.g., Khurana et al., 2004). Although the flow patterns and magnetic field configurations of the magnetosphere are different as at Earth, reconfiguration of the Jovian magnetosphere leads to reconnection

related signatures, such as dipolarizations, similar as at Earth (e.g., Artemyev et al., 2020; Kasahara et al., 2013; Kronberg et al., 2008).

Artemyev et al. (2020) presented a recent study of the Juno data in connection with ion energization during dipolarizations in Jupiter's magnetotail. They investigated the energetic heavy ion acceleration by DFs observed during six selected events. They showed a clear mass-dependent acceleration with energy of the energetic sulfur (600–7,000 keV), oxygen (500–3,500 keV), and hydrogen ions (35–900 keV) during the events. This can be explained with adiabatic ion acceleration by DFs that trap ions after their acceleration in the X-line.

However, a statistical analysis of the dependence of the DFs detected in Juno's MAG data and the ion intensity dynamics has not been conducted yet. In this paper, we investigate the relation between prominent magnetotail DF signatures, identified in the magnetic field data, and the dynamics of high-energetic ion intensities. This paper is organized as follows. In Section 2, we describe the Juno data applied in this study. In Section 3, we outline the detection method of DFs in the MAG data and provide an overview of the properties of the identified prominent signatures in the Jovian magnetotail during Juno's prime mission. Then in Sections 4 and 5, we present two DF events and describe the categorization of the DF events according to the ion intensity dynamics. In Section 6, we present the results from the statistical analysis of ion intensities, and energy spectral indices during the DF events. We finish with a summary.

2. Juno Data

In this study, we focus on the measurements of Juno's prime mission, the first 35 orbits taking place during July 2016 and July 2021. We examine the observations from the vector fluxgate magnetometer (MAG) (Connerney et al., 2017) and Juno Energetic particle Detector Instrument (JEDI) (Mauk et al., 2017) which are onboard NASA's Juno spacecraft. We use the MAG data with a time resolution of 1 s. JEDI provides electron, high-energy and low-energy ion fluxes, including ion species separation. We focus on the ion measurements of H, He, O, and S. JEDI measures the energy, angular, and compositional distributions for ions at ~20–50 keV to more than 1 MeV. We take the average ion fluxes over all angular directions. Most of the ion measurements in this study were taken when JEDI was in a low-energy-resolution mode. The energy ranges of the ion intensities are calculated from the average of the bounds of the energy passbands over the look directions in the low-energy-resolution mode. The oxygen, sulfur, and helium ion intensities are grouped to three and protons to five different energy ranges. Note that the energy bounds changed slightly in the ion measurements from the twentieth perijove (PJ), because new flight tables were uploaded to get the most performance from the instrument.

In our study, the temporal resolution of the ion intensities in each energy channel varies. We adjust the temporal resolution of the data so that almost no data gap is present in the time period of interest and that the relative error, which is obtained from the Poisson statistical error of the counts, is less than 20%. If these conditions cannot be fulfilled we discard the data of the ion species and energy channel for the particular DF event. The temporal resolution of the ion intensity data in each energy channel varies between 60 and 260 s.

The data in this study is shown in the right-handed Jupiter System III coordinates. The z axis is defined by the spin axis of Jupiter. r is pointing away from Jupiter. The longitude ϕ is parallel to the Jovigraphic equator and is measured from the positive x axis (prime meridian) in direction of the positive y axis. The colatitude θ completes the right-handed system and is positive southward.

2.1. Energy Spectral Index

The energy spectral index γ represents a slope of the ion energy spectrum $I_i \propto E_i^{-\gamma}$, where I_i is the ion intensity and E_i is the energy of the ions. γ is applied to quantify the ion energy spectra and is calculated according to Equation 6 in Kronberg and Daly (2013) by using the ion intensities for two adjacent energy channels (I_{i1} and I_{i2}) and the effective energies which are approximated by the geometric mean between the lowest energies of the channels (E_{eff_1} and E_{eff_2}):

$$\gamma = \frac{\ln(I_{i1}/I_{i2})}{\ln\left(E_{\text{eff}_2}/E_{\text{eff}_1}\right)} \tag{1}$$

γ is generally positive in the ambient environment of the magnetotail. A decrease of γ during the DF signature indicates the nonadiabatic mechanism of acceleration (see e.g., Pan et al., 2012).

3. Identification of Dipolarization Fronts in the MAG Data

We have examined the magnetic field data from Juno's prime mission, looking for a prominent positive increase of B_θ in the magnetotail at radial distances $\geq 30\ R_J$ from Jupiter. We surveyed every day of the 35 orbits identifying sharp increases in the B_θ component which stood out from the ambient perturbations of B_θ. In order to select the events of interest for our study, we apply the following selection criteria to the MAG data:

1. We select significant southward magnetic field deflections, that is, the peak of B_θ is larger than 8 nT, and declare the time of the maximum B_θ as t_{max}.
2. A minimum of B_θ ahead of t_{max} within a 5-min-long sliding window is determined. After surveying the selected events by eye, we correct the time of the minimum manually for some events. The minimum of B_θ corresponds to the start time of the DF t_{start} in our study.
3. Events which are identified during the time when Juno is located in the magnetosheath or close to the magnetopause or bow shock crossing (mostly events during PJ1 and PJ2 when Juno was located between 05:30 and 06:00 LT) according to the lists of Hospodarsky et al. (2017), Ranquist et al. (2019), and Montgomery et al. (2022) are excluded in order to focus only on internal magnetotail dynamics.
4. We require that B_θ does not have a high level of variability in a time interval of 15 min before t_{min}. Therefore, we calculate the standard deviation σ of B_θ in this interval and choose only events with $\sigma < 2.5$ nT.

During the identified events, the average background B_θ, which we define as the 10 hr running average of $|B_\theta|$ according to Vogt et al. (2020), is 3.1 nT. For each identified DF structure, we also examine the change of the elevation angle ($\Theta_{elevation} = \arctan(B_\theta/|B_r|)$) between t_{start} and t_{max}. Most events are accompanied by an increase in $\Theta_{elevation}$ of more than 25°, indicating a field reconfiguration consistent with magnetic reconnection (see e.g., Runov et al., 2021; Vogt et al., 2010). Concerning the other events, we do not evaluate $\Theta_{elevation}$ for $|B_r| < 3$ nT because then the elevation angle changes rapidly with fluctuations in B_r which might not be meaningful (see Vogt et al., 2010). With these criteria we find 87 prominent events in the MAG data for the defined period of time of the first 35 orbits of Juno. B_θ at t_{start} of the identified DFs varies between -12 and 5.1 nT with an average of 0.7 nT. The average increase of B_θ in the time $\delta t = t_{max} - t_{start}$ is about 9.6 nT. Two events show an exceptional increase up to $B_\theta = 24.7$ nT (2017 DOY 83) and $B_\theta = 33.6$ nT (2017 DOY 294) at t_{start}.

3.1. Distribution and Properties of Identified Dipolarization Fronts

Figure 1 shows the distribution of the 87 prominent DF events identified in the MAG data along with Juno's trajectory during the prime mission in the JSS (Jupiter De-Spun Sun) coordinate system. In this system, the z axis is aligned with Jupiter's spin axis but does not spin with Jupiter, the y axis is calculated from the cross product of z and the direction to the Sun, and the x axis completes the system. The events are observed in radial distances from 30 to 91 R_J, and in local time from 21:00 to 05:30 hr. It is striking that DF events identified around midnight (21:00 to 02:00 LT) are constrained to a distance less than 54 R_J to Jupiter while events identified around (pre)dawn (02:00 to 05:30 LT) are distributed between 30 and 91 R_J away from Jupiter. This distribution is in agreement with the distribution of the identified DFs in Galileo's MAG data by Kasahara et al. (2013). Using a recent data set from Juno, our investigation of the spatial distribution of prominent DFs confirms that the apparent dawn-dusk asymmetry shown by the study of Kasahara et al. (2013) is a spatial characteristic of DFs in the Jovian magnetosphere and not a feature originating from temporal changes (e.g., Io's activity). Considering the Vasyliunas cycle (Vasyliunas, 1983), the reason why more dipolarizations are observed closer to the planet at the midnight side than on the dawn side could be that reconnection is expected to arise at midnight closer to Jupiter and the X-line evolves in the tailward direction in the dawn side of the Jovian magnetotail. However, it is questionable to use the orientation of the X-line from the Vasyliunas cycle to explain the distribution of prominent DFs since the recent investigation of Juno data by Vogt et al. (2020) has shown that the Galileo X-line does not match the Juno B_θ event distribution and in contrast to the study with Galileo data (Vogt et al., 2010) they were unable to define a statistical X-line in the Juno events. Future studies of plasma flows during these events might clarify the differences between the Galileo and Juno observations.

During PJ1 and PJ2 (LT 05:30–06:00) a lot of significant perturbations in B_θ are visible. Evidence for magnetic reconnection at Jupiter's dawn magnetopause in Juno's data has been observed by Ebert et al. (2017) and
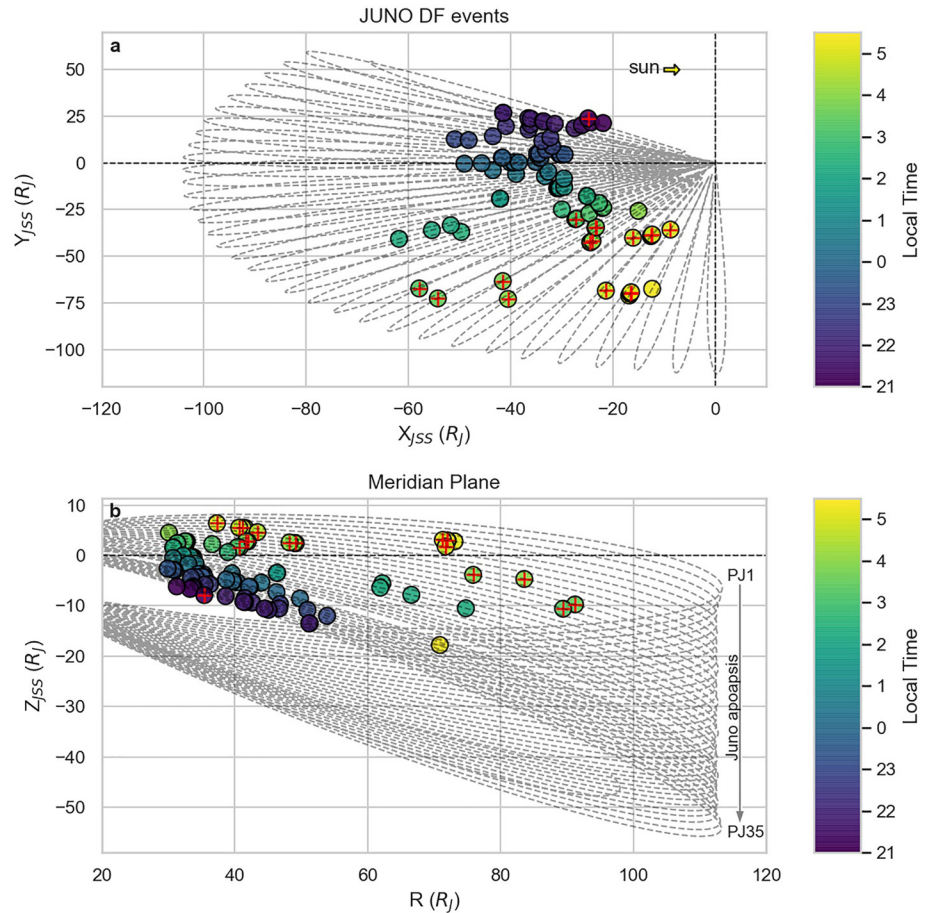
Figure 1. (a) Juno's 35 orbits (gray dashed lines) and locations of Juno during the 87 identified dipolarization front (DF) events in the MAG data (colored circles and crosses) in the Jupiter De-Spun Sun (JSS) coordinates. The sun is to the right. The colorbar of the circles gives information on the local time of each event. (b) As in panel a but in the meridian plane view. The red crosses inside the circles indicate the events which are accompanied by a decrease of the energy spectral index at least in one ion species and at one energy range. For further information see text in Section 6.3.

Montgomery et al. (2022). We exclude the significant B_θ deflections from our study because they are located at the magnetopause or in the magnetosheath (see selection criterion #3). Jupiter's magnetopause is a probable location for the development of Kelvin-Helmholtz Instabilities (e.g., Ranquist et al., 2019) which could influence the results of our study. No events which fulfill the selection criteria are identified during PJ7, PJ16, and PJ18 suggesting that the magnetospheric activity during these orbits was low, although DF events with $B_{\theta,\max} < 8$ nT can still be measured during these orbits. Vogt et al. (2020) analyzed the first 16 orbits of Juno and found about 14 reconnection events, including $B_\theta > 0$, $B_\theta < 0$, and bipolar events. They also observed that some orbits were very dynamic while others were quiet. They suggested that since consecutive orbits have nearly identical trajectories differences in magnetospheric activity from one orbit to another were due to temporal effects, such as changes in Io's plasma production or in the external solar wind conditions. On average, we identified about three prominent events per orbit. The median occurrence rate for the prominent events varies between 3 and 53 days between PJ3 and PJ20 (around 01:00–05:30 LT) and then stays almost constant at about 50 days (apart from PJ27 with 25 days). In this calculation, we do not take into account group events, which are events separated by a few hours. Group events are common especially during PJ17 (8 events), PJ11 (7 events), PJ23 (7 events), and during PJ32 (8 events). The reason for the larger occurrence period in the later orbits might be Juno's trajectory. As seen in Figure 1b, we do not observe events at higher latitudes ($z_{JSS} < -20\ R_J$).

Figure 2 shows histograms of different properties of the identified events. We find that most of the events are constrained to a radial distance of less than 50 R_J (see Figure 2a). The mean radial distance is about 44 R_J. Figure 2b shows the distribution of the events with local time. Most DF events were identified around midnight.
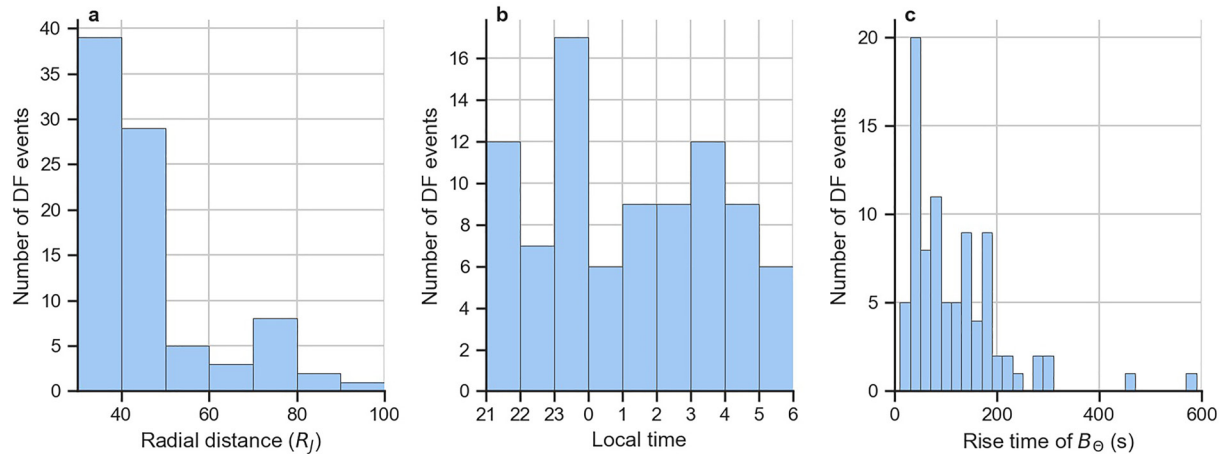
Figure 2. Histograms of different properties of the identified dipolarization front (DF) events in this study: (a) Number of DFs in observed dependence on the radial distance from Jupiter. (b) Number of DFs observed in dependence on the local time of the observations. (c) Rise time of the increase of B_θ from the minimum (beginning of the DF t_{start}) to the maximum (t_{max}) in s.

In Figure 2c) we display the rise time of the B_θ component from the minimum B_θ at t_{start} to the maximum B_θ at t_{max}. The median duration of the rise of B_θ is 84 s, the minimum duration is 13 s and maximum duration is 576 s Kasahara et al. (2013) concluded a rise time of about 60 s, although they excluded rise times over 1 min in their calculation. They showed that the average ion flow speeds at the front are in the range of 380 and 550 km/s. Given the flow speeds, the front thickness in our observations can be estimated between 0.4 R_J and 0.6 R_J. Taking the assumptions of Kasahara et al. (2013) (heavy ion dominant plasma with ion mass-per-charge ratio of 10 and the electron density of $n = 6 \times 10^{-3}$ cm^{-3}), the estimated thickness corresponds to about 3.1 c/ω_{pi} to 4.6 c/ω_{pi} with the light speed c, the ion plasma frequency ω_{pi}, and the ion inertial length c/ω_{pi}. This thickness is similar to the one calculated in the study of Kasahara et al. (2013) and larger than that at the Earth with about 1.8 c/ω_{pi} (Schmid et al., 2011). However, this estimation is very simplified since we do not have the clear ion composition for our events.

4. Case Study

In Figure 3, we present two events to show different variations of ion intensities around DFs. For each event, we show the magnetic field data (panel a), the ion intensity data (panels b–e), and the energy spectral indices (panels f–i). The prominent DFs in the two events can be recognized by a sharp increase of B_θ until a maximum ($B_\theta > 8$ nT) is reached which is marked by the black dashed lines. In Event #1, a typical $B_\theta < 0$ dip at t_{start} (see e.g., Ohtani et al., 2004) can be observed. The start of the DF structure is marked by the left edge of the gray bar. In Event #1, B_r has a similar enhancement profile than B_θ. B_r is mostly positive and experiences a reversal between 19:49 and 19:51 UTC indicating that Juno approached the current sheet center from the north. In Event #2 the magnitude of the magnetic field has a very similar profile than B_θ. B_r is very close to 0 nT at t_{start} and therefore Juno was located close to the current sheet center at the DF arrival.

Comparing the proton intensities of the two events (panel b), the intensities show different variations: In Event #1, the intensity in the low-energy population (44–73 keV) decreases shortly before the maximum while the intensities in the higher energy population increase. A similar variation can also be observed for helium intensities (panel e). The DF separates the two populations, the ambient dominant population here with energies <127 keV and the high-energy population behind the front here with energies >127 keV of the hydrogen ions (see e.g., Artemyev et al., 2020; Birn et al., 2015). The separation of the ambient dense plasma ions from the accelerated ions of the reconnection region was often observed around DFs (e.g., Birn et al., 2013, 2015; Hwang et al., 2011; Runov et al., 2009). Oxygen and sulfur intensities decrease during the DF structure in all energy channels of Event #1. The start of the decrease is around t_{start}. The energy spectral indices γ in Event #1 for hydrogen ions show a strong decrease during the DF structure at energy ranges of 56–96 and 96–187 keV, and almost no variation in γ at 392–825 keV (see panel f). γ for helium ions experiences a decrease especially in the lower energies (89–225 keV, panel i). The decrease of γ in the light ions indicates that the ions are accelerated at the front. γ for
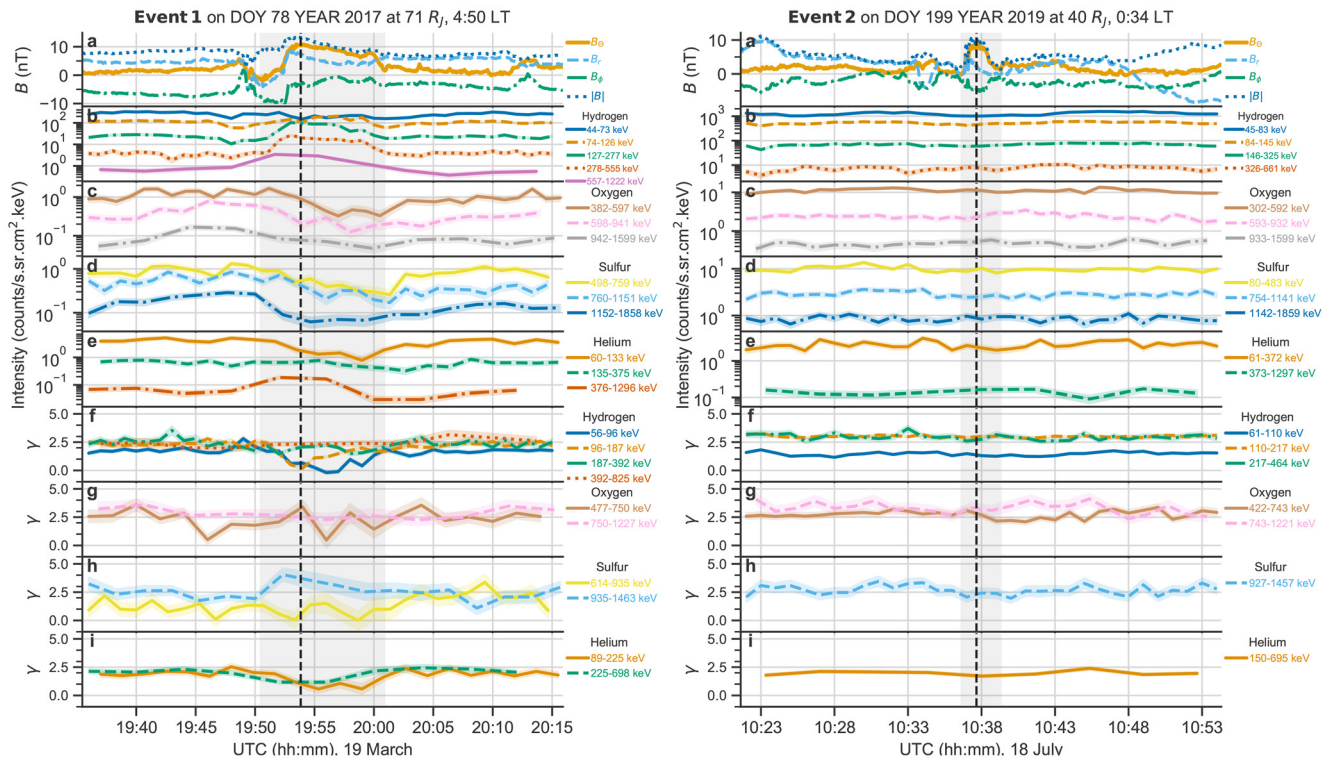
Figure 3. (a) Juno magnetometer data of the magnetic field components during the dipolarization front (DF) event on DOY 78 of 2017 (left) and on DOY 199 of 2019 (right). (b–e) Ion intensities for hydrogen, oxygen, sulfur, and helium ions at different energy channels observed with Juno Energetic particle Detector Instrument. The intensities are averaged over a sampling interval which we adjust for each ion species and energy channel separately according to the criteria given in Section 2. (f–i) Spectral indices γ calculated from the ion intensities shown in (b–e) for different energy ranges. The energy ranges represent the geometric mean between the lowest energies of the neighboring channels. The bands in panels (b–e) show the relative error obtained from the Poisson statistical error of the counts and in panels (f–i) the uncertainty in γ using error propagation of the errors in the ion intensities and Equation 1. Gray bars indicate the time of the dipolarization signature and the vertical dashed black lines indicate t_{max}. Note that the energy bounds of some energy channels are different between the two events since there was an update of the channels from spring 2019 (see Section 2).

oxygen and sulfur ions (panels g and h) strongly varies inside, before and after the DF structure in the lower energies (477–750 keV for oxygen and 614–935 keV for sulfur). γ for sulfur ions at 935–1,463 keV increases during the DF structure. During Event #2 no significant changes of all ion intensities and spectral indices at all energies is visible during the DF structure.

5. Methods for Categorization of the DF Events

The focus of our study is to investigate the dynamics of the intensity of energetic ions and the effectiveness of ion acceleration inside dipolarization structures in the Jovian magnetotail. To do so, we examine the change of ion intensity and energy spectral index in the time interval before the DF signature and inside the DF signature. In this section, we explain the categorization of the identified events. To study the correlation of the DF structure with a particular energetic ion dynamics, we introduce two different methods, which we apply for every event. One method is focused on the change of the intensity for each ion species in dependence of the energy channel and the other one is focused on the general change of intensity for each ion species in the observed energy range. In **Method 1**, we first divide the intensity variation of each ion species at each energy channel into that showing an ion intensity increase, that showing an ion intensity decrease, and that showing no change in the ion intensity. Therefore, we calculate the mean intensity of each ion species and energy channel in a time interval from t_{start} -15 min to t_{start} -5 min $\left(\overline{I}_{before}\right)$ and the minimum (I_{min}) and maximum (I_{max}) values of the ion intensity inside the DF structure in a time interval between t_{start} and t_{max} $+5$ min. This time interval allows us to capture the main features of the intensity changes due to a DF as can be seen, also later, in the superposed epoch analysis of the ion intensities shown in Figure 6. Then we analyze if the ion intensity at each energy channel during one DF event
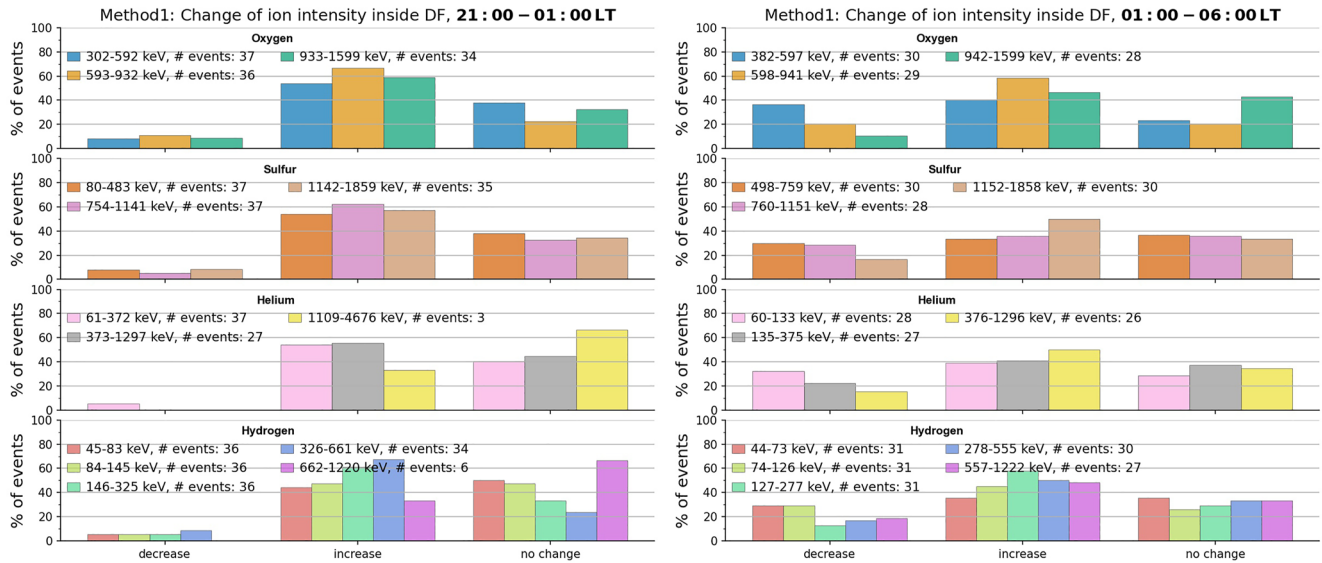
Figure 4. The histograms show the amount (in %) of dipolarization front (DF) events which are accompanied by an intensity change in different ion species and energy channels determined according to method 1 introduced in Section 5. The observations are in the midnight sector (21:00–01:00 LT, left panels) and in the (pre) dawn sector (01:00–06:00 LT, right panels). The total amount of events used for the calculation of the ion dynamics in each energy channel (given in the legend) varies because the ion intensity cannot be temporally resolved for some events and energy channels. The different colors represent different energy channels. An increase (decrease) is defined as an enhancement (decrease) of ion intensity by more than 50% from before to after the arrival of the DF.

increases by more than 50% $\left(I_{\max} / \overline{I}_{\text{before}} > 1.5 \right)$, decreases by more than 50% $\left(I_{\min} / \overline{I}_{\text{before}} < 0.5 \right)$, or does not change significantly ($0.5 \leq I_{\min} / \overline{I}_{\text{before}} \leq 1.5$ and $0.5 \leq I_{\max} / \overline{I}_{\text{before}} \leq 1.5$).

In **Method 2**, we categorize the general dynamics of intensities for each ion species during the identified DF events into four groups: (a) events with a decrease of intensity in the low-energy channels and increase in the high-energy channels (e.g., Event #1 in Figure 3, see protons and helium ions in panels b and e), (b) events with a decrease of ion intensity in at least three energy channels (e.g., Event #1 in Figure 3, see oxygen and sulfur ions in panels c and d), (c) events with an increase of ion intensity in at least three energy channels, and (d) events with no significant change of ion intensity in at least three energy channels (see Figure 3 Event #2). For the first group, we check if the ion intensity in the first energy channel decreases and increases in the third (for protons third and fourth) energy channel.

Furthermore, we require for both methods that ion intensity measurements exist during the day of the event and if two DF structures are separated by less than 20 min we consider only the first DF structure for the statistical analysis. These requirements reduce the total number of events for the ion intensity analysis from 87 to 71.

6. Statistical Results

In this section, we present the results from the statistical analysis. In Section 6.1, we display the amount of events which are accompanied by an intensity increase, intensity decrease, or no change in intensity during the DF signature in different ion species and energy channels using method 1. In Section 6.2, we show the amount of events which display a general change of the intensity in each ion species using method 2. In Section 6.3, we investigate the acceleration of ions in each event according to the decrease of the energy spectral indices.

6.1. Change of Ion Intensities in Each Energy Channel Around the DFs

Applying method 1 to the 71 identified DFs, we show the distribution of the three cases of intensity change for each ion species and energy channels in the midnight sector (21:00–01:00 LT) and in the (pre)dawn sector (01:00–06:00 LT) in the histograms in Figure 4. If the intensity at one energy range inside the DF structure is smaller (larger) than 50% compared to the intensity before the DF arrival we classify the intensity change as a decrease (an increase). Note that due to an update of the flight tables some energy boundaries are different between the observations in the midnight and (pre)dawn sector, especially for sulfur and helium (see legends in Figure 4). The time resolution of the JEDI data (see Section 2) limits the number of the total events for the
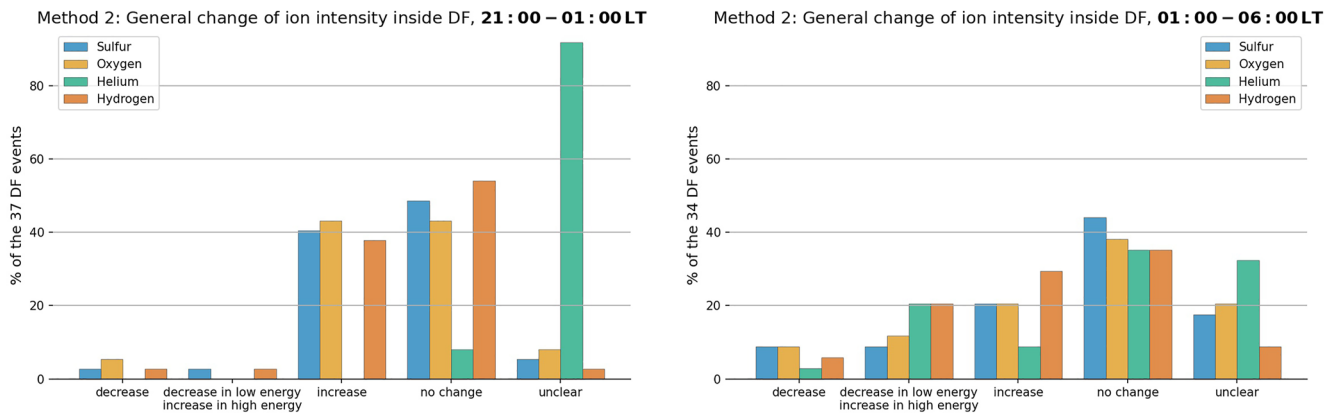
Figure 5. The histogram shows whether a dipolarization front (DF) signature is accompanied by an ion intensity change in at least three energy channels determined according to method 2 introduced in Section 5. The observations are in the midnight sector (21:00–01:00 LT, left panel) and in the (pre)dawn sector (01:00–06:00 LT, right panel). In the midnight sector, 37 events and in the dawn sector 34 events were considered for the classification. The different colors represent different ion species. "Unclear" means that the ion intensity could not be resolved in at least three energy channels for one ion species or that the event could not be classified by the criteria and therefore a conclusion about the intensity change during the DF signature could not be made.

analysis in each ion species and energy channel especially for helium and hydrogen in the highest energy channel in the midnight sector (see Figure 4 left). The total number of events in each energy range in the midnight and dawn sectors used for the analysis is given in the legends of Figure 4. The main difference of the intensity measurements during midnight and (pre)dawn is that during midnight we see less events with a decrease of the intensities for all ion species and energy channels, while in the (pre)dawn sector we do observe decreases of intensities in up to 35% of the total events. The decrease indicates that energetic ions are lost on the dawn side. The statistical analysis shows that an increase of the heavy ion intensities is observed in about 55–65% of the events in the midnight and about 35–60% of the events in the dawn sector. In the midnight sector the hydrogen (44–661 keV) and helium (61–1,297 keV) ion intensities were increased in about 45–67% of the events while in the dawn sector the hydrogen (44–1,222 keV) and helium (61–1,295 keV) ion intensities were increased in about 35–57% of the events. No significant change of the intensities is detected in about 20–49% in the both sectors.

6.2. General Change of Ion Intensities Around the DFs

The histograms in Figure 5 demonstrate whether DF signatures are accompanied by a general ion intensity change according to method 2 introduced in Section 5. In general, more than 40% of the total 71 events show no change of the proton, oxygen, and sulfur intensities during DFs. A comparison between the midnight (left panel in Figure 5) and dawn sector (right panel) show that more events without a significant change in the proton, oxygen, and sulfur intensities were observed at midnight (e.g., for protons 54% of the 37 events at midnight do not show a change in the intensities while at dawn we count only 35% of the 34 events without intensity change). More events with an increase of the heavy ion and proton intensities are observed at midnight than at dawn (e.g., about 40% of the 37 events show an increase of sulfur ion intensities at midnight and about 20% of the 34 events at dawn). An increase of ion intensities indicates that high-energetic ions are energized during these events. In more than 60% of the 71 events helium ion intensities cannot be resolved in all three energy channels especially in the midnight sector (see left panel in Figure 5) and are not applicable for our analysis. Therefore, a conclusion about the general dynamics of helium ion intensities around a DF is difficult to draw. A change of the proton intensity correlates with the same change of the oxygen and sulfur intensities in 60–95% of the events. In less than 8% of the DF events at dawn a decrease in at least three energy channels of heavy ions is observed. The distribution around a DF with a decrease of the low-energy population and an increase of the high-energy population which indicates acceleration is mostly found in the light ions (about 20% of the 34 events) at dawn shown in the right panel of Figure 5.

In Figure 6, we present the superposed epoch analysis of the ion intensities for the events where we observe a general increase according to method 2 in the proton intensities in the midnight (14 events) and dawn (10 events) sectors. The 24 events are also shown in the orange histogram in Figure 5 for the case "increase." It is visible that the variations of the intensities of protons and heavy ions are similar in the midnight sector (21:00–01:00 LT). The intensities start to increase at about 400 s before t_{max} and reach a plateau at t_{max}. Intensities at all energy
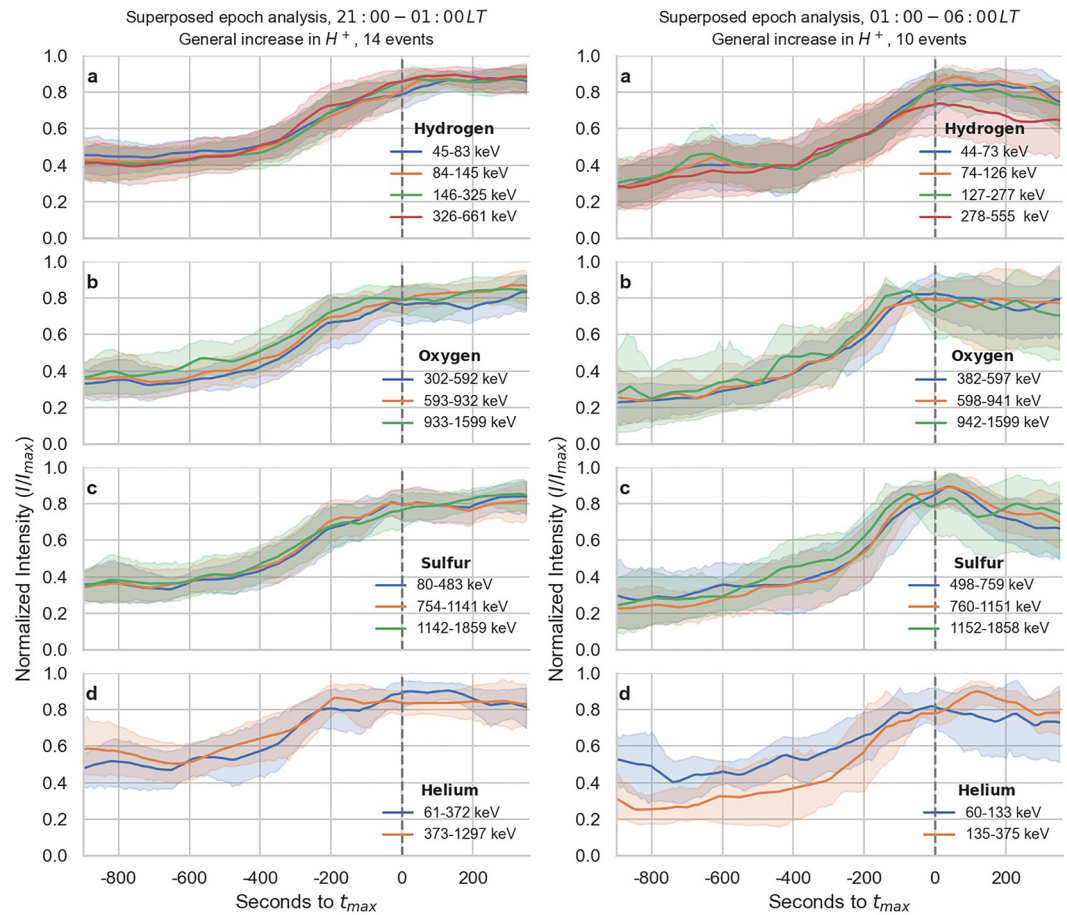
Figure 6. Superposed epoch analysis of the normalized ion intensities of the events which show a general increase in the proton intensities in the midnight (left, 14 dipolarization front (DF) events) and dawn (right, 10 DF events) sectors. The intensities are normalized by the maximum ion intensity measured during the presented time interval in each energy channel for each event. The dashed vertical line indicates the time of t_{max}. Colored bands indicate the 95% confidence interval.

ranges exhibit an increase simultaneously. However, a clear conclusion about if the increase is dispersionless in all energy channels cannot be made here due to the coarse time resolution of the data. Considering a duration of the rise of B_{θ} between t_{start} and t_{max} being <100 s (see Section 3.1), the increase of ion intensities starts about 5 min before the start of the DFs. A similar observation especially for light ions at Earth's magnetotail was shown by Malykhin et al. (2019). They also showed that γ for light ions started to decrease almost simultaneously with the intensity increase before the start of the DFs. They explained the dynamics with a nonadiabatic acceleration mechanism where the light ions are reflected and accelerated by the approaching front and moving ahead of it (see Zhou et al., 2010). The statistical analysis of γ (not shown here) for the events with a general increase of the ion intensities shown in Figure 4 does not reveal a significant change.

Due to the large error bar in the helium intensities in the midnight and dawn sector, the intensity increase is not significant during the DFs. In the dawn sector, the confidence intervals are larger because we have less events for the analysis in this local time range. The heavy ion intensities show a more pronounced peak in the dawn sector already 100 s before t_{max} for oxygen ions and sulfur ions (in the energy range of 1,152–1,858 keV). The intensities are normalized by the maximum value of the intensity in the considered time range in each event. We notice that the intensities of protons and heavy ions after DF arrival are on average 3 times larger than the intensities prior to the DF in the midnight sector, while in the dawn sector they are on average 6 times larger.
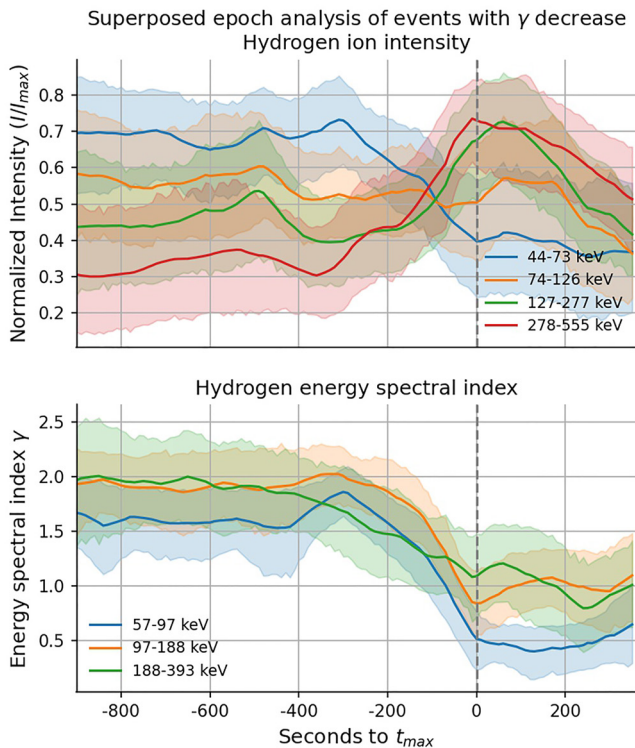
Figure 7. Superposed epoch analysis of the normalized proton intensity and energy spectral indices γ of the events where a decrease of γ in at least one energy range of the protons was observed (in total 12 events). All events are observed in the dawn sector. The intensities are normalized by the maximum ion intensity measured during the presented time interval in each energy channel for each event. The dashed vertical line indicates the time of t_{max}. Colored bands indicate the 95% confidence interval. The energy ranges displayed in the second panel are the geometric means between the lowest energies of the neighboring channels. For better visibility, we do not show the normalized intensity in the energy range of 557–1,222 keV and γ in the energy range of 393–825 keV.

6.3. Decrease of the Energy Spectral Index Around DF

We are interested to see if acceleration of energetic ions is present around the identified DFs. Therefore, we look for a significant decrease of γ inside the DFs which is an indication for nonadiabatic ion acceleration. For the statistical analysis of γ for different ion species and energy ranges around the DF, we compare the minimum value (γ_{before}) in the time interval of $t_{min} -15$ min and $t_{min} -5$ min before the DF arrival and the minimum value (γ_{inside}) during DF in the time interval of t_{min} and $t_{max} +5$ min. We declare a significant decrease of γ when γ decreases inside the DF by more than 50% compared to the γ before the DF arrival (i.e., $\gamma_{inside}/\gamma_{before} < 0.5$). We find 16 events where γ is decreased at least in one ion species and in one energy range in the dawn sector and one event in the midnight sector. In Figure 1, we show the locations of these events in the Jovian magnetotail as red crosses. The events are not constrained to a radial distance but they are all located close to the Jovigraphic equator. Almost all of the events are observed in the dawn sector between 03:00 and 05:00 LT. Out of the 16 events with a significant decrease of γ in the dawn sector, 12 events show a decrease of γ in the energy range of 57–97 keV of the protons. That means that in about 40% of the events observed in the dawn sector, we detect a decrease of γ in the 57–97 keV range. In the midnight sector, we find only one event with a decrease of γ for protons out of 36 observed events. A superposed epoch analysis of the normalized proton intensities and γ for protons of these 12 events in the dawn sector is shown in Figure 7. It is visible that the decrease of γ starts at around 300 s before t_{max} and continues until t_{max}. After t_{max} γ stays almost constant. The decrease of γ is stronger for the lower energy range (57–97 keV) than for the higher energy ranges. We see a significant decrease of γ from 1.9 ± 0.2 to 0.6 ± 0.3 at t_{max} in the energy range of 57–97 keV. An apparent decrease of γ for higher energy ranges (>188 keV) is not significant since the confidence intervals are large. The superposed epoch analysis of the proton intensities shows that we observe ion acceleration mostly in the events where the intensity of the low-energy population (<127 keV) decreases and the high-energy population (>127 keV) increases. Furthermore, a significant decrease of γ in at least one energy range is observed in 14 events for the sulfur ions, 9 events for the oxygen ions, and 8 events for the helium ions.

7. Summary and Discussion

In this study, we used Juno's MAG and JEDI observations of the prime mission (first 35 orbits) and investigated the dynamics of the ion intensities, ion energization and acceleration around DFs in the Jovian magnetotail. First, we identified 87 prominent DF (peak $B_\theta > 8$ nT) events in the MAG data. Further requirements for the ion intensity data reduced the total number of events for the ion intensity analysis from 87 to 71. Then we have examined the statistical properties of oxygen, sulfur, helium, and hydrogen ion intensities observed with JEDI and spectral indices inside the DFs and in a time interval before the DF arrival. Our statistical analysis yielded the following results:

1. Our results confirm the findings from Galileo data of Kasahara et al. (2013) that the prominent events are distributed at around 30–90 R_J on the dawnside while events at the midnight side are concentrated near Jupiter (<54R_J). Since the apparent dawn-dusk asymmetry is observed in two independent data sets it is most likely a spatial and not a temporal characteristic of the prominent events in the Jovian magnetosphere. Assuming ion flow speeds of 380–550 km/s we estimated a front thickness of about 0.4–0.6 R_J.

2. The comparison of the ion intensity observations during DFs at the dawn side and midnight side shows that less events with a decrease of the ion intensities are located at the midnight side, while in the (pre)dawn sector we do observe decreases of intensities in up to 12 events. Particularly, an increase of the oxygen and hydrogen ion intensities in one energy channel (O: 593–932 keV, H: 326–661 keV) can be observed in up to 67% of the

events on the midnight side. In up to 50% (H: 45–83 keV) of the events on the midnight side no significant variation of the ion intensities is observed. For the case where the DFs are accompanied by a general increase of the ion intensities, the intensity increase during the DFs is on average two times higher at the dawn sector than at the midnight sector.

3. In more than 40% of 71 DF events no significant change is observed in the ion intensity dynamics for protons, oxygen, and sulfur ions. More events without a significant change in the proton, oxygen, and sulfur intensities are located in the midnight sector (e.g., for protons 20 events at midnight do not show a change in the intensities while at dawn 12 events are observed without intensity change). About 30% of the 71 events are accompanied by an increase of energetic particle intensities indicating high-energetic ion energization. Less than 12% of the 71 DF events mostly located in the dawn sector showed similar variations of the ion intensity often observed around a DF in Earth's magnetotail with a decrease of the ambient dominant population and increase of the high-energy population around a DF which indicates ion acceleration.

4. A significant decrease of the energy spectral index inside the DFs in at least one ion species and energy range is observed in 16 DF events indicating ion acceleration during the DFs. Almost all of these events are located close to the Jovigraphic equator and between 03:00 LT and 05:00 LT. Particles which did not get lost but stayed trapped by the DF might have had more time to be accelerated on the dawn side since reconnected flux tubes might have traveled from the midnight side tailward on the dawnside. The ion intensities during these events show a decrease in the low-energy channel and increase in the high-energy channels. The change of the intensities and energy spectral indices start almost simultaneously already before the start of the DFs.

We have shown that some DF events were accompanied by ion intensity variations and some were not. In our study, we did not find any clear correlation between different properties of the DFs and ion intensity variations. Therefore, the question on the link between DFs and dynamics of energetic ions remain unanswered. Similar findings were also presented for the Earth's magnetosphere by Liu et al. (2016) and Runov et al. (2021, 2022). Liu et al. (2016) showed that one of the differences between a DF event with a significant increase (injection) and no significant change of the ion intensities is the DF duration: DFs with enhanced intensities rise in about 10 s, whereas DFs without intensity variations rise in about 20 s. In our analysis, we do not see a clear dependence between the rise time duration of the front and intensity variations during the DFs. Liu et al. (2016) also observed a significant difference in the electric field for events with and without energetic particle injections. The electric field magnitude was larger for events with injections suggesting that injections result from a DFs electric field directly accelerating the particles.

A closer look on the electron behavior during the events where no change of ion intensities was observed as well as on the JADE observations of ions with lower energies could be useful for further analysis. A better temporal resolution of the particle data, analysis of the electric fields and available ion plasma moments would be helpful for further investigations of the energetic ion dynamics inside DFs.

Data Availability Statement

The Juno data can be found on the Planetary Data System at https://pds-ppi.igpp.ucla.edu/. Juno MAG data used in this study are the 1-s PC files from data set "JNO-J-3-FGM-CAL-V1.0" (https://doi.org/10.17189/1519711). Juno JEDI data are from the data set "JNO-J-JED-3-CDR-V1.0" (https://doi.org/10.17189/1519713). The data analysis was done with Python using SciPy and seaborn packages among others.

References

Angelopoulos, V., Baumjohann, W., Kennel, C. F., Coroniti, F. V., Kivelson, M. G., Pellat, R., et al. (1992). Bursty bulk flows in the inner central plasma sheet. *Journal of Geophysical Research*, *97*(A4), 4027–4039. https://doi.org/10.1029/91JA02701

Artemyev, A. V., Clark, G., Mauk, B., Vogt, M. F., & Zhang, X. J. (2020). Juno observations of heavy ion energization during transient dipolarizations in Jupiter magnetotail. *Journal of Geophysical Research: Space Physics*, *125*, e27933. https://doi.org/10.1029/2020JA027933

Birn, J., Hesse, M., Nakamura, R., & Zaharia, S. (2013). Particle acceleration in dipolarization events. *Journal of Geophysical Research: Space Physics*, *118*, 1960–1971. https://doi.org/10.1002/jgra.50132

Birn, J., Runov, A., & Hesse, M. (2015). Energetic ions in dipolarization events. *Journal of Geophysical Research: Space Physics*, *120*, 7698–7717. https://doi.org/10.1002/2015JA021372

Connerney, J. E. P., Benn, M., Bjarno, J. B., Denver, T., Espley, J., Jorgensen, J. L., et al. (2017). The Juno magnetic field investigation. *Space Science Reviews*, *213*(1–4), 39–138. https://doi.org/10.1007/s11214-017-0334-z

Ebert, R. W., Allegrini, F., Bagenal, F., Bolton, S. J., Connerney, J. E. P., Clark, G., et al. (2017). Accelerated flows at Jupiter's magnetopause: Evidence for magnetic reconnection along the dawn flank. *Geophysical Research Letters*, *44*, 4401–4409. https://doi.org/10.1002/2016GL072187

Fu, H., Grigorenko, E. E., Gabrielse, C., Liu, C., Lu, S., Hwang, K. J., et al. (2020). Magnetotail dipolarization fronts and particle acceleration: A review. *Science China Earth Sciences*, *63*(2), 235–256. https://doi.org/10.1007/s11430-019-9551-y

Hospodarsky, G. B., Kurth, W. S., Bolton, S. J., Allegrini, F., Clark, G. B., Connerney, J. E. P., et al. (2017). Jovian bow shock and magnetopause encounters by the Juno spacecraft. *Geophysical Research Letters*, *44*, 4506–4512. https://doi.org/10.1002/2017GL073177

Hwang, K.-J., Goldstein, M. L., Lee, E., & Pickett, J. S. (2011). Cluster observations of multiple dipolarization fronts. *Journal of Geophysical Research*, *116*, A00132. https://doi.org/10.1029/2010JA015742

Jackman, C. M., Thomsen, M. F., Mitchell, D. G., Sergis, N., Arridge, C. S., Felici, M., et al. (2015). Field dipolarization in Saturn's magnetotail with planetward ion flows and energetic particle flow bursts: Evidence of quasi-steady reconnection. *Journal of Geophysical Research: Space Physics*, *120*, 3603–3617. https://doi.org/10.1002/2015JA020995

Kasahara, S., Kronberg, E. A., Kimura, T., Tao, C., Badman, S. V., Masters, A., et al. (2013). Asymmetric distribution of reconnection jet fronts in the Jovian nightside magnetosphere. *Journal of Geophysical Research: Space Physics*, *118*, 375–384. https://doi.org/10.1029/2012JA018130

Kasahara, S., Kronberg, E. A., Krupp, N., Kimura, T., Tao, C., Badman, S. V., et al. (2011). Magnetic reconnection in the Jovian tail: X-Line evolution and consequent plasma sheet structures. *Journal of Geophysical Research*, *116*, A11219. https://doi.org/10.1029/2011JA016892

Khurana, K., Kivelson, M., Vasyliunas, V., Krupp, N., Woch, J., Lagg, A., et al. (2004). Jupiter. the planet, satellites and magnetosphere. In *The configuration of Jupiter's magnetosphere* (pp. 593–616). Cambridge University Press.

Kronberg, E. A., & Daly, P. W. (2013). Spectral analysis for wide energy channels. *Geoscientific Instrumentation, Methods and Data Systems*, *2*(2), 257–261. https://doi.org/10.5194/gi-2-257-2013

Kronberg, E. A., Kasahara, S., Krupp, N., & Woch, J. (2012). Field-aligned beams and reconnection in the Jovian magnetotail. *Icarus*, *217*(1), 55–65. https://doi.org/10.1016/j.icarus.2011.10.011

Kronberg, E. A., Woch, J., Krupp, N., Lagg, A., Daly, P. W., & Korth, A. (2008). Comparison of periodic substorms at Jupiter and Earth. *Journal of Geophysical Research*, *113*, A04212. https://doi.org/10.1029/2007JA012880

Liu, J., Angelopoulos, V., Zhang, X.-J., Turner, D. L., Gabrielse, C., Runov, A., et al. (2016). Dipolarizing flux bundles in the cis-geosynchronous magnetosphere: Relationship between electric fields and energetic particle injections. *Journal of Geophysical Research: Space Physics*, *121*, 1362–1376. https://doi.org/10.1002/2015JA021691

Liu, J., Angelopoulos, V., Zhou, X.-Z., & Runov, A. (2014). Magnetic flux transport by dipolarizing flux bundles. *Journal of Geophysical Research: Space Physics*, *119*, 909–926. https://doi.org/10.1002/2013JA019395

Malykhin, A. Y., Grigorenko, E. E., Kronberg, E. A., Daly, P. W., & Kozak, L. V. (2019). Acceleration of protons and heavy ions to suprathermal energies during dipolarizations in the near-Earth magnetotail. *Annales Geophysicae*, *37*(4), 549–559. https://doi.org/10.5194/angeo-37-549-2019

Mauk, B. H., Haggerty, D. K., Jaskulek, S. E., Schlemm, C. E., Brown, L. E., Cooper, S. A., et al. (2017). The Jupiter energetic particle detector instrument (JEDI) investigation for the Juno mission. *Space Science Reviews*, *213*(1–4), 289–346. https://doi.org/10.1007/s11214-013-0025-3

Montgomery, J., Ebert, R. W., Clark, G., Fuselier, S. A., Allegrini, F., Bagenal, F., et al. (2022). Investigating the occurrence of magnetic reconnection at Jupiter's dawn magnetopause during the Juno era. *Geophysical Research Letters*, *49*, e2022GL099141. https://doi.org/10.1029/2022GL099141

Nakamura, R., Baumjohann, W., Klecker, B., Bogdanova, Y., Balogh, A., Rème, H., et al. (2002). Motion of the dipolarization front during a flow burst event observed by cluster. *Geophysical Research Letters*, *29*, 31–34. https://doi.org/10.1029/2002GL015763

Ohtani, S.-i., Shay, M. A., & Mukai, T. (2004). Temporal structure of the fast convective flow in the plasma sheet: Comparison between observations and two-fluid simulations. *Journal of Geophysical Research*, *109*, A03210. https://doi.org/10.1029/2003JA010002

Pan, Q., Ashour-Abdalla, M., El-Alaoui, M., Walker, R. J., & Goldstein, M. L. (2012). Adiabatic acceleration of suprathermal electrons associated with dipolarization fronts. *Journal of Geophysical Research*, *117*, A12224. https://doi.org/10.1029/2012JA018156

Ranquist, D. A., Bagenal, F., Wilson, R. J., Hospodarsky, G., Ebert, R. W., Allegrini, F., et al. (2019). Survey of Jupiter's dawn magnetosheath using Juno. *Journal of Geophysical Research: Space Physics*, *124*, 9106–9123. https://doi.org/10.1029/2019JA027382

Runov, A., Angelopoulos, V., Henderson, M. G., Gabrielse, C., & Artemyev, A. (2021). Magnetotail dipolarizations and ion flux variations during the main phase of magnetic storms. *Journal of Geophysical Research: Space Physics*, *126*, e2020JA028470. https://doi.org/10.1029/2020JA028470

Runov, A., Angelopoulos, V., Sitnov, M. I., Sergeev, V. A., Bonnell, J., McFadden, J. P., et al. (2009). Themis observations of an earthward-propagating dipolarization front. *Geophysical Research Letters*, *36*, L14106. https://doi.org/10.1029/2009GL038980

Runov, A., Angelopoulos, V., Weygand, J. M., Artemyev, A. V., Beyene, F., Sergeev, V., et al. (2022). Thin current sheet formation and reconnection at x ∼ -10r_E during the main phase of a magnetic storm. *Journal of Geophysical Research: Space Physics*, *127*, e2022JA030669. https://doi.org/10.1029/2022JA030669

Schmid, D., Volwerk, M., Nakamura, R., Baumjohann, W., & Heyn, M. (2011). A statistical and event study of magnetotail dipolarization fronts. *Annales Geophysicae*, *29*(9), 1537–1547. https://doi.org/10.5194/angeo-29-1537-2011

Smith, A. W., Jackman, C. M., Thomsen, M. F., Sergis, N., Mitchell, D. G., & Roussos, E. (2018). Dipolarization fronts with associated energized electrons in saturn's magnetotail. *Journal of Geophysical Research: Space Physics*, *123*, 2714–2735. https://doi.org/10.1002/2017JA024904

Sundberg, T., Slavin, J. A., Boardsen, S. A., Anderson, B. J., Korth, H., Ho, G. C., et al. (2012). Messenger observations of dipolarization events in mercury's magnetotail. *Journal of Geophysical Research*, *117*, A00M03. https://doi.org/10.1029/2012JA017756

Vasyliunas, V. M. (1983). Plasma distribution and flow. In A. J. Dessler (Ed.) *Physics of the Jovian magnetosphere* (pp. 395–453). Cambridge University Press.

Vogt, M. F., Connerney, J. E., DiBraccio, G. A., Wilson, R. J., Thomsen, M. F., Ebert, R. W., et al. (2020). Magnetotail reconnection at Jupiter: A survey of Juno magnetic field observations. *Journal of Geophysical Research: Space Physics*, *125*, e2019JA027486. https://doi.org/10.1029/2019JA027486

Vogt, M. F., Kivelson, M. G., Khurana, K. K., Joy, S. P., & Walker, R. J. (2010). Reconnection and flows in the Jovian magnetotail as inferred from magnetometer observations. *Journal of Geophysical Research*, *115*, A06219. https://doi.org/10.1029/2009JA015098

Xu, S. B., Huang, S. Y., Yuan, Z. G., Deng, X. H., Jiang, K., Wei, Y. Y., et al. (2021). Global spatial distribution of dipolarization fronts in the Saturn's magnetosphere: Cassini observations. *Geophysical Research Letters*, *48*, e2021GL092701. https://doi.org/10.1029/2021GL092701

Yao, Z. H., Grodent, D., Ray, L. C., Rae, I. J., Coates, A. J., Pu, Z. Y., et al. (2017). Two fundamentally different drivers of dipolarizations at Saturn. *Journal of Geophysical Research: Space Physics*, *122*, 4348–4356. https://doi.org/10.1002/2017JA024060

Yao, Z. H., Radioti, A., Grodent, D., Ray, L. C., Palmaerts, B., Sergis, N., et al. (2018). Recurrent magnetic dipolarization at Saturn: Revealed by Cassini. *Journal of Geophysical Research: Space Physics*, *123*, 8502–8517. https://doi.org/10.1029/2018JA025837

Zhou, X.-Z., Angelopoulos, V., Sergeev, V. A., & Runov, A. (2010). Accelerated ions ahead of earthward propagating dipolarization fronts. *Journal of Geophysical Research*, *115*, A00I03. https://doi.org/10.1029/2010JA015481